High Efficiency Refrigeration and Pyroelectric Energy Harvesting Applications of Lead Titanate Based Relaxer Ceramic

Tianfu Zhang (ztf143@163.com)
Xinyang Normal University
Xianxiong Huang
Guangdong University of Technology
Hu Xu
Guangdong University of Technology
Shujie Sun
Xianyang Normal University
Zuodong Liu
Xinyang Normal University
Xin-Gui Tang
Guangdong University of Technology

Research Article

Keywords: Ceramics, dielectric, relaxer, electrocaloric

Posted Date: September 28th, 2020

DOI: https://doi.org/10.21203/rs.3.rs-82746/v1

Abstract

Relaxer ferroelectrics are highly attractive in electrocaloric due to large breakdown electric field and wide phase transition temperatures, which has great potential applications in solid-state cooling. In this work, relaxer ferroelectrics are synthesized by a traditional solid state reaction method. Phase transition and relaxer characteristics are studied by temperature dependent dielectric spectrums. Temperature dependent ferroelectric properties are also studied to calculate electrocaloric effect. Maximum value of refrigeration efficiency η (ΔT/ΔE) is about 0.079 K·cm/kV, our result lays a foundation and provides a reference for studying high efficiency solid-state electrocaloric refrigeration. Pyroelectric energy harvesting are studied, maximum pyroelectric energy harvesting is 279 kJ/cm 3 .

Introduction

Refrigeration is indispensable in our daily life, such as: food preservation, air conditioning, medical aspects (organ refrigeration, organ transplantation), microelectronic refrigeration, and *etc* [1, 2]. The refrigeration method of the common compressor has almost reached its limit, the organic gas it discharged directly destroys the olfactory oxygen layer causing the global greenhouse effect, environmental damage appeals more and more attention recently. As a result, finding a new way of cooling method becomes an urgent task.

The unique properties and great variety of relaxer ferroelectrics make them highly attractive [3]. During the past decades, intensive research efforts have been conducted to develop solid-state cooling technologies [4, 5]. Electrocaloric effect (*ECE*) is the isothermal entropy change (ΔS) and adiabatic temperature change (ΔT) of polar materials during application and removal of electric field, which is more environmental friendly and satisfies the demand of realizing next-generation solid-state cooling devices for various applications [4], the operation schematics of electrocaloric cooling technology is shown in Figure 1. Recently, relaxer ferroelectrics for future solid-state refrigeration technologies become very hot [6, 7], high energy conversion efficiency, easy miniaturization, wide temperature region of phase transitions and large breakdown electric field indicate the potential applications in solid-state refrigeration technologies.

It is a well-known fact that thin films have advantages in small solid state cooling devices, but bulk materials play an important role on larger scale devices [8]. As a result, *ECE* of bulk materials are desired, we should pay more attentions to *ECE* of bulk materials. Bulk materials including multilayer capacitors, ceramics and single crystals have been reported a lot, such as: PMN-PT single crystal [9], PLZT multilayer capacitors [10], $Ba(Ti,Ce)O_3$-$(Ba,Ca)TiO_3$ ceramics [11], PLZT ceramics [12], and *etc*. Compared to multilayer capacitors and single crystals, ceramics have the advantages of low-cost and easier fabrications [13]. As a result, *ECE* of ceramics are important.

$(Pb_{0.91}La_{0.09})(Hf_{0.65}Ti_{0.35})_{0.9775}O_3$ (PLHT) and $(Pb_{0.91}La_{0.09})(Zr_{0.65}Ti_{0.35})_{0.9775}O_3$ (PLZT) ceramics are prepared and studied. Frequencies and temperatures dependent dielectric permittivity ε_γ and loss *tanδ* are also investigated to study the relaxer phase transitions and defects related relaxations. Great *ECE* results

are achieved, maximum value of ΔT is about 1.96 K, maximum value of refrigeration efficiency is η ($\Delta T/\Delta E$) is about 0.079 K·cm/kV, the huge refrigeration efficiency η and large reversible adiabatic temperature change ΔT indicate that applications in future solid-state refrigeration devices.

Experimental

Ceramic samples of PLHT and PLZT were prepared by a conventional solid state reaction method using high-purity raw materials Pb_3O_4, La_2O_3, ZrO_2, HfO_2, and TiO_2 (AR, Macklin Biochemical Co., Ltd., China). The powders were weighed based on nominal composition and mixed in ethanol using zirconia balls for 12 h. The mixture was ball-milled for 24 h after calcination at 900 ^oC for 3 h, the green body was sintered at 1300 ^oC for 5 h. The sintered sample discs were polished into a thickness of 0.5 mm, and then the two parallel surfaces were covered with silver paste and finally fired at 600 ^oC for 30 min as electrodes.

Dielectric characteristic was conducted by an impedance analyzer (VDMS-2000H, Partulab, Wuhan, China) with the heating rate of 3^oC/min. Ferroelectric hysteresis loops (*P-E*) and current density-electric field (*I–E*) curves were tested by using a ferroelectric tester (TZFE-300, Harbin Julang Technology Co., Ltd., Harbin, China) with a frequency of 10 Hz. Structure of PLHT and PLZT ceramics was analyzed by X-ray diffraction (XRD; Bruker D2 PHASER, Germany). The surface morphologies of PLHT and PLZT were determined by field-emission scanning electron microscope (FE-SEM; S 4800, Hitachi, Japan).

Results And Discussions

Figure 2 shows XRD patterns of PLHT and PLZT ceramics. Several obvious diffraction peaks are observed from XRD patterns, namely (100), (110), (111), (200), (210), (211) and (220), indicating that all sintered ceramics exhibit stable perovskite structures. The inset of Fig. 2 displays SEM images of PLHT and PLZT bulk ceramics. The samples possess dense and homogeneous microstructures with only few visible pores.

Temperature dependent dielectric permittivity ε_r and loss *tanδ* of PLHT and PLZT ceramics are shown in Figs. 3a-b. In lower temperature region (≤150 ^oC), both loss *tanδ* and permittivity ε_r exhibit single independent peak clearly for PLZT and PLHT ceramics, which are due to the phase transition of ferroelectric→paraelectric phase, similar results are also reported [14]. Maximum permittivity ε_r appears around 405.15 K, and 355.15 K respectively for PLZT and PLHT ceramics. From Fig. 3, T_m (temperature of maximum ε_r) shift to higher temperatures with increasing frequencies, but maximum values of dielectric permittivity ε_r decrease with increasing frequencies, this phenomenon indicates typical relaxer behaviors.

Dielectric relaxation usually denotes reorientational processes in condensed matter that can be detected by dielectric spectroscopy [15]. Generally speaking, while temperature is above Curie temperature, then permittivity ε_r of a normal ferroelectric usually is suitable for the Curie-Weiss law, and dielectric

characteristics can be described by equation [16]: $1/\varepsilon_\gamma=(T-T_o)/C$, $(T>T_C)$, where T_o and C are Curie-Weiss temperature and Curie-Weiss constant, respectively. Permittivity ε_γ of PLHT and PLZT ceramics are studied by the Curie-Weiss law, plots of temperature dependent inverse $10000/\varepsilon_\gamma$ (at 10 kHz) are shown in Figs. 3c-d (Black quadrate, the solid black lines are used to fit the Curie-Weiss law). Clearly, T_o are about 483.15 K and 421.15 K respectively for PLZT and PLHT ceramics. Besides dielectric behaviors of relaxer ferroelectrics usually deviate from the typical Curie-Weiss behavior, as a result, dielectric relaxer characteristics can be described by a modified Curie-Weiss relationship [17, 18]: $1/\varepsilon_\gamma-1/\varepsilon_m=(T-T_m)^\gamma/C_1$, $(1\leq\gamma\leq2)$, where γ and C_1 are constant. The character of phase transitions can be revealed by parameter γ. The plots of $\ln(1/\varepsilon_\gamma-1/\varepsilon_m)$ versus $\ln(T-T_m)$ with (at 10 kHz) (Blue quadrate, the solid blue lines are used to fit the modified Curie-Weiss law) are shown in Fig. 3. Values of parameter γ = 1.92 and 1.79 respectively for PLZT and PLHT ceramics obtained by by modified Curie-Weiss relationship. Fitting values of γ also support relaxer characteristics in PLHT and PLZT ceramics.

In order to calculate *ECE* of PBLZST ceramics, *P-E* loops and *I-E* curves of PLZT and PLHT ceramics under various temperatures are shown in Figs. 4a-b, with increasing measured temperatures, *P-E* loops appear to be typical relaxer ferroelectric loops, which indicates the relaxer nature, saturation polarization decreases sharply with increasing temperatures. *I-E* curves provide detailed picture of phase switching process, a single sharp current peak is observed in the *I-E* curves, which can be attributed to the domain switching. Flat *I-E* curves with two split current peaks can be observed in PLHT ceramics, indicating the higher composition of nonpolar phase. The transition from short-range nonergodic relaxer ferroelectric to long-range metastable ferroelectric phase can be disassembled by two parts: the generation of micro-sized domains from PNRs that embedded in the easily polarized matrix, and the alignment of the micro-sized domains driven by high electric field. As a result, the two current peaks in the *I-E* curves can be ascribed to the formation of micro-sized domains and the domain switching under further applied electric field [19].

According to the principle of *ECE*, when electric field increases from E_1 to E_2, the isothermal entropy change ΔS of an *ECE* material should be: $\Delta S=S(E_1,T)-S(E_2,T)$. Therefore, initial conditions of *ECE* materials at E_1 (in most cases, E_1=0) will affect *ECE* directly. Assuming the Maxwell relation: $(\partial P/\partial T)_E=(\partial S/\partial E)_T$. The corresponding isothermal entropy change ΔS and the reversible adiabatic temperature change ΔT are calculated by following relations [20]: $\Delta S=-1/\rho\cdot\int(\partial P/\partial T)_E dE$, $\Delta T=-T/C\rho\cdot\int(\partial P/\partial T)_E dE$, where ρ, C, E_1 and E_2 are mass density, mass heat capacity, initial and final applied electric fields, respectively. Values of $(\partial P/\partial T)_E$ is the pyroelectric coefficient at the applied electric field and can be obtained from the numerical differentiation of polarization-temperature data, which are extracted from upper branches of *P-E* loops ($E>0$) measured at various temperatures. ΔS and ΔT calculated at different electric fields are presented in Figs. 4c-d. Both ΔS and ΔT show humps near phase transition temperatures. On the other hand, ΔT increase continuously with increasing measured electric fields. Maximum positive *ECE* are 1.96 K and 1.24 K respectively for PLZT and PLHT ceramics. For solid-state refrigeration technologies applications, the quantitative effect of electric field ΔE on ECE of dielectrics is also desired, refrigeration

efficiency is $\eta=\Delta T/\Delta E$ [21]. Maximum values of refrigeration efficiency is η ($\Delta T/\Delta E$) is about 0.079 K·cm/kV for PLZT ceramics, which is much higher than previous reports in $BaHfTiO_3$ ceramic [6], NBBST thin film [22], BNBT/BCZT bilayer [23], $BaTiO_3$-based ceramics [24], $PbSrTiO_3$ ceramics [25], PBLZT anti-ferroelectric thick film [26].

Ferroelectrics have been widely studied in energy harvesting applications due to the outstanding pyroelectric characteristics which are promising to convert heat fluctuations into electrical energy. Pyroelectric effect reflects the variation of spontaneous polarization in pyroelectric material with changing temperatures [27]. Significant variations of polarization under different temperatures induce giant pyroelectric energy harvesting density (N_D), which can be estimated by using Olsen cycle between two hysteresis loops [28]. A complete Olsen cycle (A→B→C→D→A) consists of two isothermal (A→B and C→D) and two isoelectric (B→C and D→A) process in Fig.5a. Energy conversion in these processes have been described in elsewhere [29]. The output electrical energy density N_D per cycle in Fig.5a is calculated by the following formula [27]: , where E and P are electric field and polarization respectively, it is numerically equal to green shaded area in Fig.5a. In this work, the maximum pyroelectric energy harvesting are 279 and 234 kJ/cm^3 respectively for PLZT and PLHT ceramic with ΔT = 90°C (shown in Fig. 5b). Our results shows higher values than previous reports in PZT ceramic [30], BZT-50BCT ceramic [31], $SrBaNb_2O_6$ ferroelectric ceramics [32], and *etc*.

Conclusion

In this work, PLZT and PLHT ceramics are synthesized by a traditional solid state reaction method, and pure phase is obtained from XRD spectrum of all sintered samples. Phase transition behaviors and relaxer characteristics are studied. Maximum reversible adiabatic temperature change ΔT are 1.96 K and 1.24 K respectively for PLZT and PLHT ceramics, maximum value of refrigeration efficiency is η ($\Delta T/\Delta E$) is about 0.079 K·cm/kV, the current progresses achieved in this work show potential applications for solid-state refrigeration devices. Maximum pyroelectric energy harvesting values are 279 and 234 kJ/cm^3 respectively for PLZT and PLHT ceramic.

Declarations

ACKNOWLEDGEMENT

This work was supported by Nanhu Scholars Program for Young Scholars of XYNU.

CONFLICT OF INTEREST

The authors declare that they have no conflict of interests.

References

1. Li L, Xu M, Zhang Q*, et al*. Electrocaloric effect in La-doped BNT-6BT relaxor ferroelectric ceramics. *Ceramics International* 2018, **44**(1): 343-350.
2. Alpay SP, Mantese J, Trolier-McKinstry S*, et al*. Next-generation electrocaloric and pyroelectric materials for solid-state electrothermal energy interconversion. *MRS Bulletin* 2014, **39**(12): 1099-1111.
3. Prah U, Rojac T, Wencka M*, et al*. Improving the multicaloric properties of $Pb(Fe_{0.5}Nb_{0.5})O_3$ by controlling the sintering conditions and doping with manganese. *Journal of the European Ceramic Society* 2019, **39**(14): 4122-4130.
4. Zhang G, Fan B, Zhao P*, et al*. Ferroelectric Polymer Nanocomposites with Complementary Nanostructured Fillers for Electrocaloric Cooling with High Power Density and Great Efficiency. *ACS Applied Energy Materials* 2018, **1**(3): 1344-1354.
5. Manosa L, Planes A. Materials with Giant Mechanocaloric Effects: Cooling by Strength. *Advanced materials* 2017, **29**(11): 1603607.
6. Li J, Zhang D, Qin S*, et al*. Large room-temperature electrocaloric effect in lead-free $BaHf_xTi_{1-x}O_3$ ceramics under low electric field. *Acta Materialia* 2016, **115**: 58-67.
7. Liu Y, Scott JF, Dkhil B. Direct and indirect measurements on electrocaloric effect: Recent developments and perspectives. *Applied Physics Reviews* 2016, **3**(3): 031102.
8. Scott JF. Electrocaloric Materials. *Annual Review of Materials Research* 2011, **41**(1): 229-240.
9. Zhang TF, Tang XG, Ge PZ*, et al*. Orientation related electrocaloric effect and dielectric phase transitions of relaxor PMN-PT single crystals. *Ceramics International* 2017, **43**(18): 16300-16305.
10. Zhao Y, Hao X, Zhang Q. Enhanced energy-storage performance and electrocaloric effect in compositionally graded $Pb_{(1-3x/2)}La_xZr_{0.85}Ti_{0.15}O_3$ antiferroelectric thick films. *Ceramics International* 2016, **42**(1): 1679-1687.
11. Yang Y, Zhou Z, Ke X*, et al*. The electrocaloric effect in intrinsic-acceptor-doped $Ba(Ti,Ce)O_3$-$(Ba,Ca)TiO_3$ ceramics. *Scripta Materialia* 2020, **174**: 44-48.
12. Zhao YC, Liu QX, Tang XG*, et al*. Giant Negative Electrocaloric Effect in Anti-Ferroelectric $(Pb_{0.97}La_{0.02})(Zr_{0.95}Ti_{0.05})O_3$ Ceramics. *ACS Omega* 2019, **4**(11): 14650-14654.
13. Zhang TF, Huang XX, Tang XG*, et al*. Enhanced electrocaloric analysis and energy-storage performance of lanthanum modified lead titanate ceramics for potential solid-state refrigeration applications. *Scientific Reports* 2018, **8**(1): 396.
14. Fu C, Chen Q, Cai W*, et al*. Microstructure and Dielectric Properties of La-doped Barium Titanate Hafnate Ceramics. *Integrated Ferroelectrics* 2012, **139**(1): 7-13.
15. Kabir E, Khatun M, Mustafa RJ*, et al*. AC electrical conductivity and dielectric properties of doping induced molecular ferroelectric diisopropylammonium bromide. *Materials Research Express* 2019, **6**(9): 096306.
16. Li J, Li J, Qin S*, et al*. Effects of Long- and Short-Range Ferroelectric Order on the Electrocaloric Effect in Relaxor Ferroelectric Ceramics. *Physical Review Applied* 2019, **11**(4): 044032.

17. Jayakrishnan AR, Alex KV, Thomas A*, et al*. Composition-dependent x$Ba(Zr_{0.2}Ti_{0.8})O_3$-(1-x) $(Ba_{0.7}Ca_{0.3})TiO_3$ bulk ceramics for high energy storage applications. *Ceramics International* 2019, **45**(5): 5808-5818.
18. Lan Z, Liu J, Ren S*, et al*. Phase evolution and relaxor behavior of BiScO3–$PbTiO_3$–$0.05Pb(Yb_{1/2}Nb_{1/2})O_3$ ternary ceramics. *Journal of Materials Science* 2019, **54**(21): 13467-13478.
19. He H, Lu X, Li M*, et al*. Thermal and compositional driven relaxor ferroelectric behaviours of lead-free $Bi_{0.5}Na_{0.5}TiO_3$-$SrTiO_3$ ceramics. *Journal of Materials Chemistry C* 2020, 8: 2411-2418
20. Peng B, Zhang M, Tang S*, et al*. Frequency dependent electrocaloric effect in Nb-doped PZST relaxor thin film with the coexistence of tetragonal antiferroelectric and rhombohedral ferroelectric phases. *Ceramics International* 2020, **46**(4): 4300-4306.
21. Huang F, Tian H, Meng X*, et al*. Large Room Temperature Electrocaloric Effect in $KTa_{1-x}Nb_xO_3$ Single Crystal. *physica status solidi (RRL) - Rapid Research Letters* 2019, **13**(2). 1800515
22. Yang C, Han Y, Feng C*, et al*. Toward Multifunctional Electronics: Flexible NBT-Based Film with a Large Electrocaloric Effect and High Energy Storage Property. *ACS Applied Materials & Interfaces* 2020, **12**(5): 6082-6089.
23. Shirsath SE, Cazorla C, Lu T*, et al*. Interface-Charge Induced Giant Electrocaloric Effect in Lead Free Ferroelectric Thin-Film Bilayers. *Nano Letters* 2020, **22**(2): 1262-1271.
24. Lv Z, Wei J, Yang T*, et al*. Manipulation of Curie temperature and ferroelectric polarization for large electrocaloric strength in $BaTiO_3$-based ceramics. *Ceramics International* 2020, **46**(10): 14978-14984.
25. Ge P-Z, Jian X-D, Lin X-W*, et al*. Composition dependence of giant electrocaloric effect in $Pb_xSr_{1-x}TiO_3$ ceramics for energy-related applications. *Journal of Materiomics* 2019, **5**(1): 118-126.
26. Gao H, Hao X, Zhang Q*, et al*. Thickness-dependent electrocaloric effect of $Pb_{0.82}Ba_{0.08}La_{0.10}(Zr_{0.90}Ti_{0.10})O_3$ antiferroelectric thick films. *Journal of Alloys and Compounds* 2017, **690**: 131-138.
27. Siao AS, McKinley IM, Chao CK*, et al*. Pyroelectric waste heat energy harvesting using the Olsen cycle on Pb(Zr,Ti)O_3-Pb(Ni,Nb)O_3 ceramics. *Journal of Applied Physics* 2018, **124**(17): 174104.
28. Vats G, Vaish R, Bowen CR. An analysis of lead-free $(Bi_{0.5}Na_{0.5})_{0.915}$-$(Bi_{0.5}K_{0.5})_{0.05}Ba_{0.02}Sr_{0.015}TiO_3$ ceramic for efficient refrigeration and thermal energy harvesting. *Journal of Applied Physics* 2014, **115**(1): 013505.
29. Vats G, Kumar A, Ortega N*, et al*. Giant pyroelectric energy harvesting and a negative electrocaloric effect in multilayered nanostructures. *Energy Environ Sci* 2016, **9**(4): 1335-1345.
30. Patel S, Chauhan A, Vaish R. Enhanced energy harvesting in commercial ferroelectric materials. *Materials Research Express* 2014, **1**(2): 025504.
31. Vats G, Chauhan A, Vaish R. Thermal Energy Harvesting Using Bulk Lead-Free Ferroelectric Ceramics. *International Journal of Applied Ceramic Technology* 2015, **12**: E49-E54

32. Tang H, Tang XG, Li MD, *et al*. Pyroelectric energy harvesting capabilities and electrocaloric effect in lead-free $Sr_xBa_{1-x}Nb_2O_6$ ferroelectric ceramics. *Journal of Alloys and Compounds* 2019, **791**: 1038-1045.

Figures

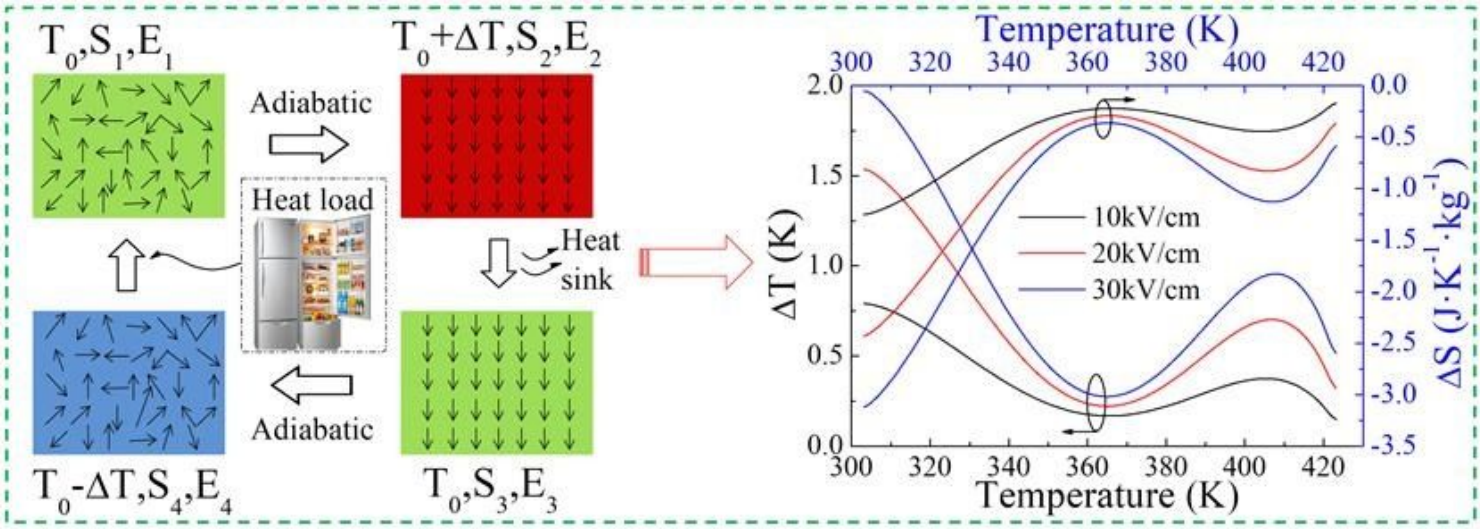

Figure 1

Operation schematics of electrocaloric cooling technology.

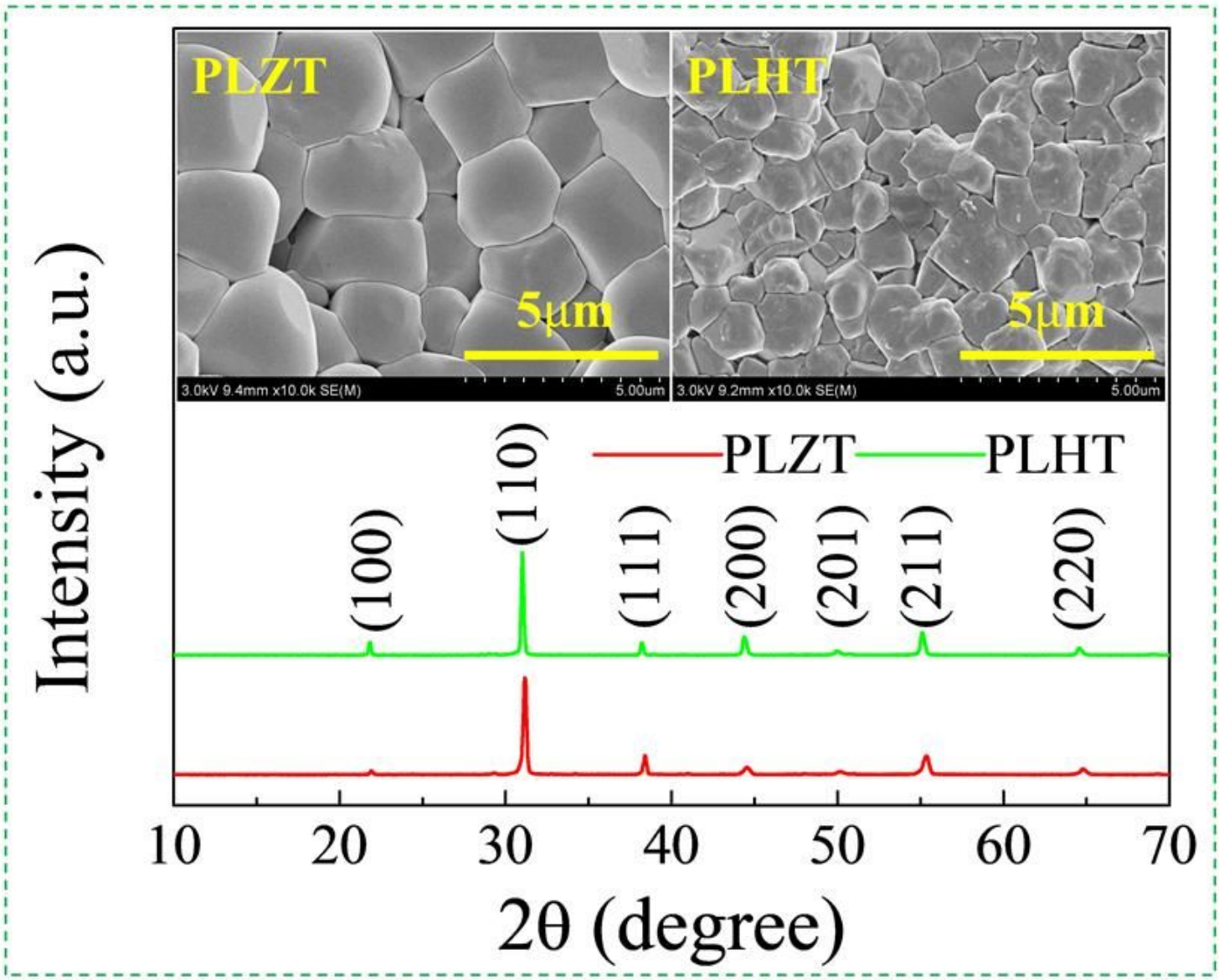

Figure 2

XRD patterns of PLZT and PLHT ceramics. Insets show SEM images of PLZT and PLHT ceramics.

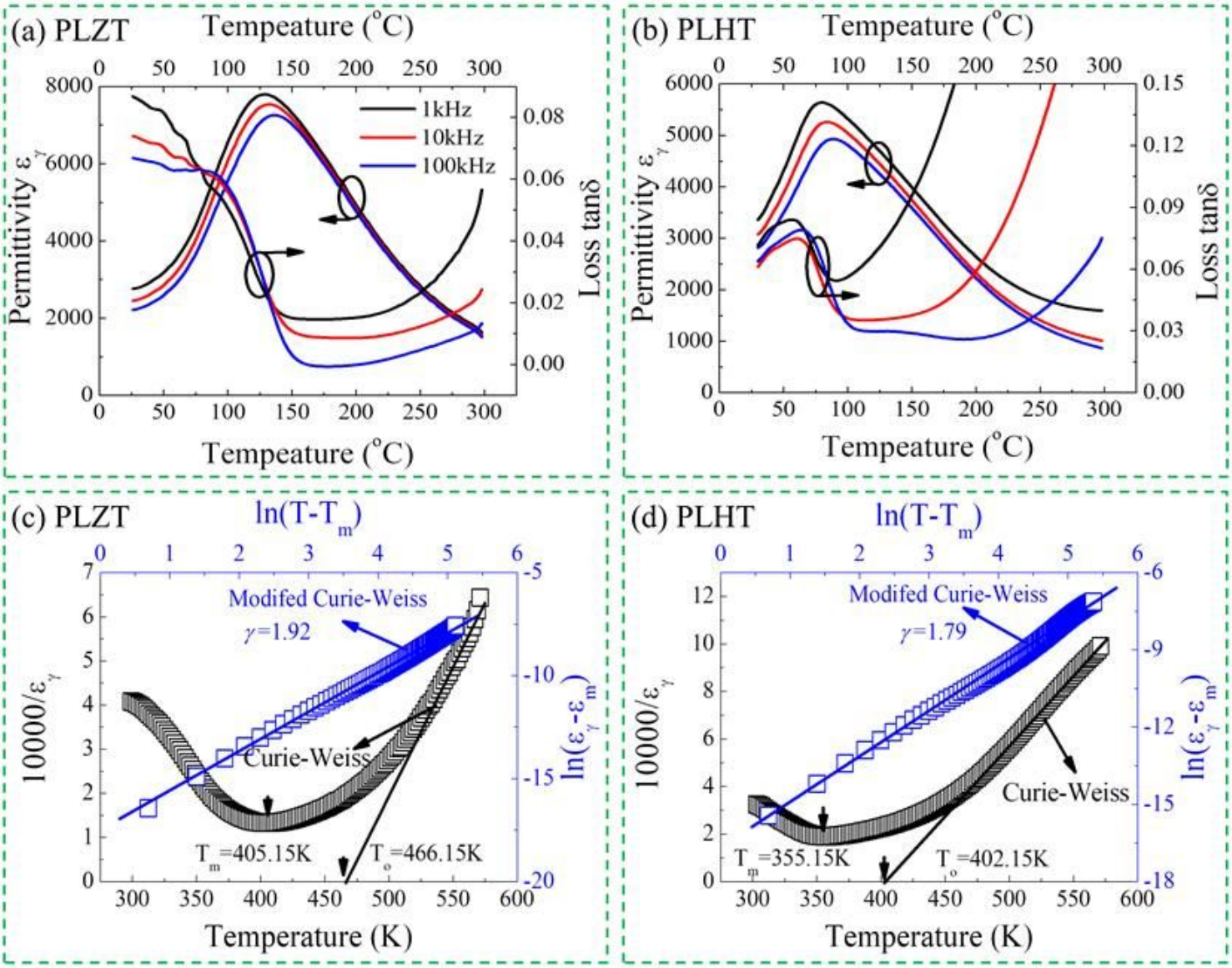

Figure 3

Permittivity εγ and loss tanδ as a function of temperature for PLZT (a) and PLHT (b) ceramics measured at different frequencies (1, 10, and 100 kHz), the inverse dielectric permittivity (10000/εγ) as a function of temperature (The solid lines are used to fit by the Curie-Weiss law) and plots of ln(1/εγ-1/εm) as a function of ln(T-Tm) for PLZT (c) and PLHT (d) ceramics.

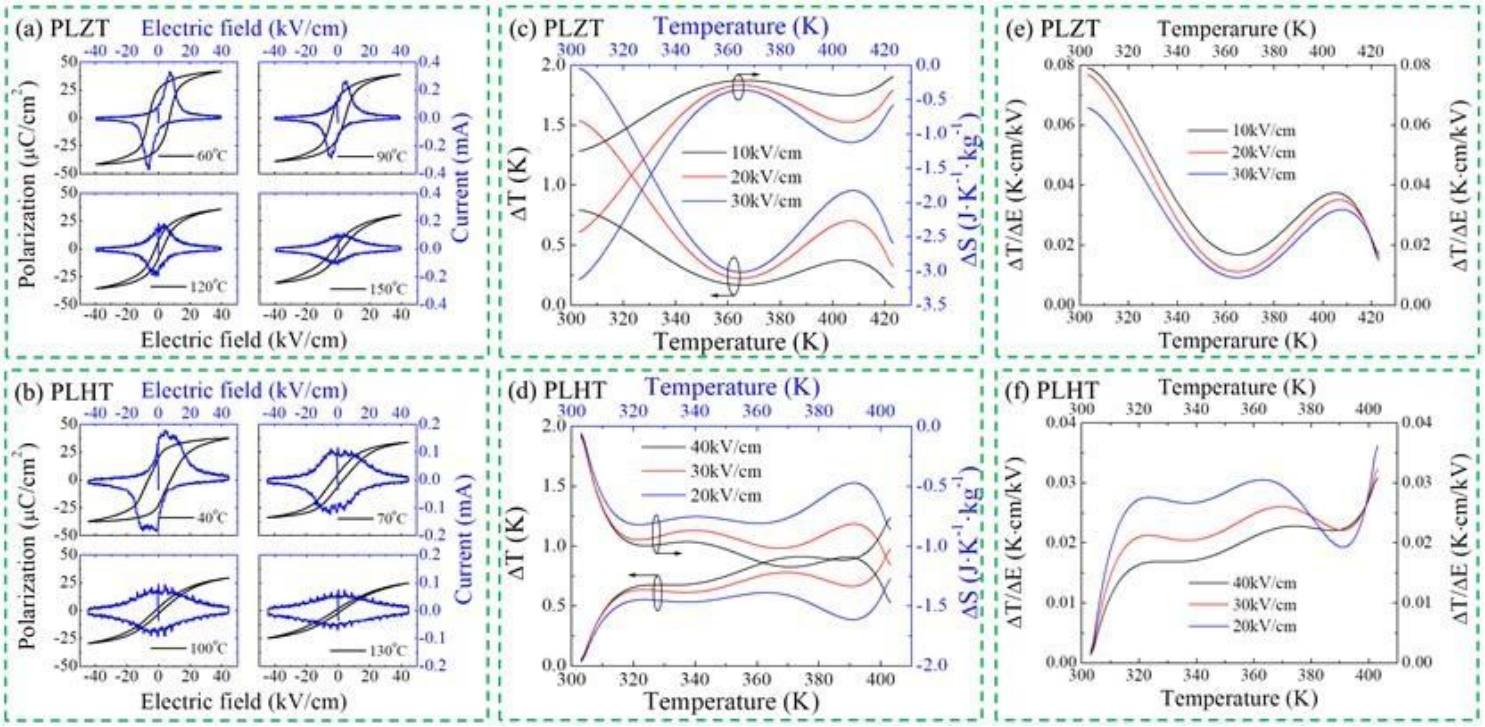

Figure 4

P-E loops and I-E curves of PLZT (a) and PLHT (b) ceramics measured at 10 Hz under various temperatures, reversible adiabatic temperature change ΔT of PLZT (c) and PLHT (d), refrigeration efficiency η of PLZT (e) and PLHT (f).

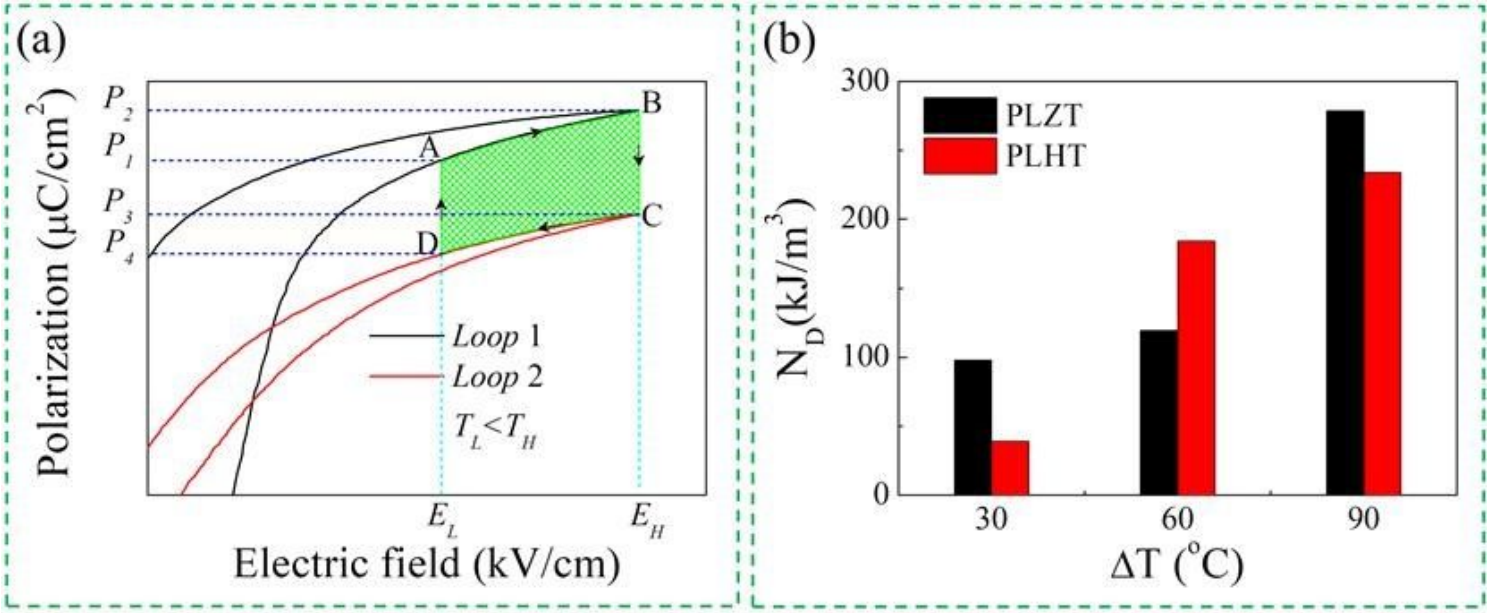

Figure 5

The principle of pyroelectric energy harvesting using the Olsen cycle (a) and pyroelectric energy harvesting density per cycle as a function of ΔT (b).

Supplementary Files

This is a list of supplementary files associated with this preprint. Click to download.

- renamed1e03d.TIF